ISSN 1808-8546 (ONLINE) 1808-3765 (CD-ROM)

AVALIAÇÃO DE PROTÓTIPOS DE SENSORES DE RADIAÇÃO SOLAR DE BAIXO CUSTO PARA ESTIMATIVA DA EVAPOTRANSPIRAÇÃO POTENCIAL

JULIANA SÁNCHEZ BENÍTEZ; LUCIANO SOBRAL FRAGA JUNIOR; ALISSON MACENDO AMARAL E LUCAS MELO VELLAME

[1]Faculdade de Engenharia Agrícola, Universidade Estadual de Campinas, Cidade Universitária "Zeferino Vaz", CEP 13083-970, Campinas, São Paulo, Brasil, j218736@dac.unicamp.br.
[2]Dr. em Engenharia de sistemas agrícolas, ESALQ/USP, lucianosobral@alumni.usp.br
[3]Instituto Federal do Norte de Minas Gerais - Campus Arinos, Rodovia MG 202, Km 407, 38680000 - Arinos, MG – Brasil.
[4]Centro de Ciências Agrárias, Ambientais e Biológicas, Universidade Federal do Recôncavo da Bahia, rua Rui Barbosa, 710, Campus Universitário CEP 74690900, Cruz das Almas, Bahia, Brasil, lucasvellame@gmail.com

1 RESUMO

O cálculo da evapotranspiração de referência pelo método da FAO 56 necessita de dados da radiação solar, o qual pode ser medido ou estimado. O alto valor dos sensores traz a necessidade do uso de equações como a equação de *Hargraves-Samani.* Objetivou-se construir e avaliar um piranômetro de baixo custo e fácil reprodução, baseado no uso de um fotodiodo de silício. Foram construídos e testados 16 sensores por um período de 414 dias. Entre os principais resultados desta pesquisa destaca-se a incerteza do instrumento para estimar radiação global de ± 0,04 MJ $m^{-2}dia^{-1}$, os desvios na estimativa da ETo_{PM} foram inferiores a 0,22 $mmdia^{-1}$ em 95% das observações realizadas, esses desvios são 3,62 vezes menores que os desvios na estimativa da radiação usando a equação de *Hargraves-Samani* com calibração local e mesma probabilidade de ocorrência. O período necessário para a calibração com 99,7% de confiança foi de 32 dias. O sensor tem custo total aproximado de US$ 27,23. Os resultados demonstram que o sensor pode ser utilizado em estações meteorológicas automatizadas, instaladas em campo aberto ou em ambiente protegido, com acurácia suficiente para estimativas de ETo_{PM} de baixo custo.

Palavras-chave: piranômetro de baixo custo, irradiância, sensor de baixo custo, evapotranspiração.

SÁNCHEZ-BENÍTEZ, J.; FRAGA JUNIOR, L. S.; AMARAL, A. M.; VELLAME, L. M.;
EVALUATION OF LOW-COST SOLAR RADIATION PROTOTYPES TO ESTIMATE POTENTIAL EVAPOTRANSPIRATION

2 ABSTRACT

To calculate the reference evapotranspiration by the FAO56 method (EToPM) solar radiation shall be measured or estimated. Due to the high value of sensors, equations such as the Hargraves-Samani equations are used. The objective of this project was to build and evaluate a low-cost and easy-to-reproduce pyranometer. Sixteen sensors were built and tested for 414

Recebido em 21/06/2021 e aprovado para publicação em 30/08/2022
DOI: http://dx.doi.org/10.15809/irriga.2022v27n3p607-623

days. Among the main results of this research highlights that the uncertainty of the instrument to estimate global radiation of ±0.04 MJ m-² day-1, deviations in the EToPM estimate was less than 0.22 mm day-1 in 95% of the observations performed, these deviations are 3.62 times smaller than the deviations caused by the radiation estimate using the Hargraves-Samani equation with local calibration and same probability of occurrence. The period required for calibration for 99.7% confidence was 32 days. The sensor has an approximately total cost of $27.23. The results demonstrate that the sensor can be used in automated weather stations, installed in the open field or in a protected environment, with sufficient accuracy for low-cost EToPM estimates.

Keywords: Low cost pyranometer, irradiance, low cost sensor, evapotranspiration.

3 INTRODUCTION

The study of solar radiation can be performed for various purposes, including meteorology, hydrology, agriculture, and other engineering fields. One such application is the estimation of evapotranspiration (ET), which is usually performed to determine the water requirements of a crop for irrigation planning and management purposes (RAFI *et al.*, 2019). Owing to the great difficulty of estimating ET via direct field measurements, in 1990, the FAO proposed a standard method for estimating reference evapotranspiration (ETo) via the *Penman–Monteith equation*, which is based on temporal data from a meteorological station and can be manual or automated (BORNHOFEN, 2015).

An automated synoptic meteorological station (AMS) is characterized by energy autonomy and data collection and transmission at established time intervals (MAPA, 2011). The sensors commonly used in conventional AMSs have installation costs that are inaccessible to many rural producers, extension workers, and researchers, which motivates the development of low-cost meteorological stations. Some AMSs are available on the national market and are built with sensors made from locally available components, allowing them to be sold at lower costs than imported sensors.

The development of sensors and the popularization of the use of low-cost weather stations is growing in Brazil, but the pyranometer is still an instrument that is rarely supplied by the national industry (VILELA, 2010). Despite the development of several studies in the country that have proposed easily reproducible and low-cost pyranometers (FREIRE, 2008; VILELA, 2010; BOLZAN, 2014), the availability of measured solar radiation data remains limited. This leads, in many cases, to dispensing with the pyranometer to measure solar radiation and relying on mathematical models such as *the Hargreaves-Samani model*, which estimates solar radiation on the basis of air temperature variations (BORGES *et al.*, 2010).

There are two types of pyranometers: thermopiles and silicon photodiodes. The latter is an economical alternative to thermal pyranometers, despite their limited response to the solar radiation spectrum. A photodiode is a sensor commonly used in infrared detection applications, remote control data transmission systems, photometers, or infrared optical control applications in industry. The photodiode offers the advantage of its electromagnetic spectrum measurement range, which is within the highest sensitivity zone of thermal pyranometers, for pyranometer construction. Another advantage is its rapid, virtually instantaneous response to changes in radiation intensity (GÓMEZ *et al.*, 2018).

As a disadvantage, this type of sensor degrades more quickly than a thermopile sensor. Amorphous silicon solar cells undergo degradation within the first few months of operation, reducing their performance over their lifetime (SILVA, 2015).

The present work aimed to evaluate the employability of a pyranometer built with low-cost materials in the estimation of ETo via the *Penman–Monteith model* through its integration with the sensors of a meteorological station.

4 MATERIALS AND METHODS

4.1 Construction of sensors

The construction of the photovoltaic pyranometers was based on an adaptation of the methodology presented by Freire (2008). The sensor consists of a silicon photodiode connected in parallel to a 33 Ω resistor and fixed inside a ½-inch black threaded sleeve (Figure 1A). Two ½-inch polyvinyl chloride (PVC) caps were threaded onto the ends of the sleeve. The upper end cap was used as a light filter, limiting the radiation range reaching the measuring element (Figure 1C), and the lower end cap was used to support the other components.

Figure 1 Step-by-step construction of the photovoltaic pyranometer sensor.

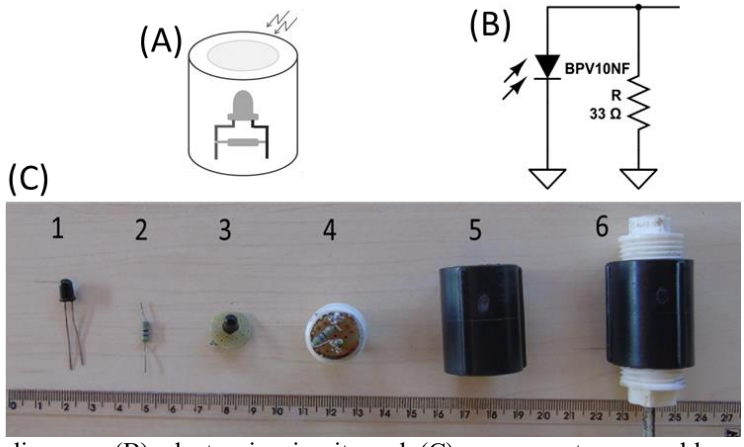

(A) Sensor operating diagram, (B) electronic circuit, and (C) pyranometer assembly sequence. In (C), (1) corresponds to the photodiode, (2) is the 33 Ω resistor, (3) is the sensor and resistor soldered on a universal prototype board, (4) the assembly soldered and joined to the threaded plug, (5) the PVC sleeve with thread correction, and (6) the union of all parts forming the sensor. **Source:** The authors (2021).

4.2 Photodiode selection

Initially, two pyranometer prototypes were built with the aim of selecting the best prototype. Photodiodes of the BPW20RF and BPV10NF models were used as measuring elements. Compared with that of the BPV10NF model, which has a sensitivity range that varies between 790 and 1050 nm and a sensitivity angle of ± 20°, the sensitivity range of the BPW20RF model varies from 400 to 1100 nm and is characterized by a wide incident light capture angle of ± 50° (VISHAY, 2011) (VISHAY, 2019). Compared with commercial pyranometer sensors such as the Campbell SC® CS300 sensor, which covers a sensitivity range between 360 and 1120 nm (CAMPBELL SCIENTIFIC, 2018), the Campbell SC® LP02 thermal pyranometer, which covers a wider sensitivity range, from 285 to 3000 nm (CAMPBELL SCIENTIFIC, 2012), has smaller measurement ranges and angles of incidence.

To select the sensing element, data collection was performed under full sunlight conditions, with two prototypes placed on a horizontal bar 2 m high and levelled in a northerly direction to avoid shading between the pyranometers. A secondary thermopile pyranometer, Campbell SC® LP02, was used as the standard pyranometer for comparison purposes. The instruments (prototypes and standards) were connected to a Campbell Sci® CR1000 data acquisition system, and measurements were taken every 30 seconds. Averages were stored at five-minute intervals for five days.

4.3 Sensor calibration

Sensor calibration was performed according to the 1990 ISO 6090 standard (INTERNATIONAL ORGANIZATION FOR STANDARDIZATION, 1990), which refers to the calibration of the experimental device against a standard device. The reference device should be a secondary standard thermopile pyranometer such as the LP02 (ISO9060:2018, *Campbell SC*®). The calibration process consists of performing a mathematical model to correlate the voltage response of the photovoltaic pyranometer with the irradiance response of the reference sensor.

The experiment was conducted at the Federal University of Recôncavo da Bahia (UFRB) in the city of Cruz das Almas-BA, located at the geographic coordinates Latitude: 12° 39' 29.4" South, Longitude: 39° 5' 45" West. Sixteen low-cost sensors were built using the BPV10NF photodiode and fixed to a metal bar 2 m above the ground, positioned north and perpendicular to the sun's rays, over a homogeneous pasture in a tree-free terrain (Figure 2). In addition to the standard sensor, a commercial photovoltaic pyranometer (CS300 - Campbell SC®) was added.

All the sensors were connected to a CR1000 *datalogger* (Campbell SC®) for data collection and storage. Sensor signal data (mV) were collected between April 13, 2018, and June 1, 2019, with an observation interval of 30 seconds and averages stored every 15 minutes. The data sampling period was established to minimize differences caused by the thermal inertia of the sensors since they have different operating principles. For the LP02 sensor (thermopile), the response time is less than 18 s (CAMPBELL SCIENTIFIC, 2012), and for the CS300 sensor (photodiode), it is less than 1 s (CAMPBELL SCIENTIFIC, 2018).

Figure 2. Sensors located above the horizontal bar at the beginning of the data collection period under open field conditions between 04/13/2018 and 06/01/2019.

Source: The authors (2018).

After completing the open-field data sampling, the calibration structure and sensors were installed inside a greenhouse to calibrate the sensors for a protected environment. The test station was installed in the experimental area of the same university (latitude: 12° 39' 22" South, longitude: 39° 5' 16.5" West) from November 1, 2019, to December 10, 2019. The same data collection and storage unit was used, which was programmed to store average values every 15 minutes.

4.3 Measurement uncertainty

Measurement uncertainty is defined as an indicator of how much the estimated value differs from the true value of the measurand in terms of probability and is estimated as the 95% confidence interval for measurements (INMETRO, 2012b). The standard uncertainty of low-cost pyranometers was calculated according to the INMETRO methodology (INMETRO, 2012a) (Equation 1).

$$\sigma = \sqrt{\frac{\sum_{j=1}^{k}(\overline{yJ}-y_j)^2}{k-1}} \quad (1)$$

where σ is the standard uncertainty; k is the number of observed points; y_j represents each of the observations made with the low-cost pyranometer; and $\overline{yJ}$ represents the value of observations made with the standard LP02 pyranometer.

From the standard uncertainty of the instrument, the minimum number of observations required to guarantee reliability and reduce the field calibration time can be estimated, thus optimizing the calibration time of new sensors (INMETRO, 2012a) (Equation 2).

$$n = (\frac{3\,\sigma}{le})^2 \quad (2)$$

where n is the number of observations used to estimate the statistical error limit, σ is the standard uncertainty of the instrument, and le is the limit of statistical error 99.7%.

4.5 Estimation of reference evapotranspiration

To evaluate the usability of low-cost sensors for estimating the atmospheric evaporative demand, the reference evapotranspiration (ETo $_{PM}$) was calculated via the *Penman–Monteith* model suggested by Allen *et al.* (1998) (Equation 3). The estimated solar radiation data obtained with each of the 16 low-cost sensors and the CS300 sensor during the open-field calibration period were used.

$$ETo = \frac{0{,}408\,\Delta(Rn-G)+\gamma\frac{900}{T+273}u_2(e_s-e_a)}{\Delta+\gamma(1+0{,}34u_2)} \quad (3)$$

where ETo is the reference evapotranspiration (MJ m $^{-2}$ day $^{-1}$); Rn is the net radiation at the crop surface (MJ m $^{-2}$ day $^{-1}$); G is the heat flux (MJ m $^{-2}$ day $^{-1}$); T is the average air temperature (°C); u_2 is the average wind speed at a height of 2 m (ms $^{-1}$); e_s is the saturation vapor pressure (kPa); e_a is the current vapor pressure (kPa); $(e_s - e_a)$ is the vapor pressure deficit (kPa); Δ is the slope of the vapor pressure curve (kPa °C^{-1}); and Υ is the psychrometric constant (kPa °C^{-1}).

The other meteorological data required for the ETo calculation were obtained from the metrological station that monitored the development of the experiment (thermohygrometer HC2S3L12, anemometer 03002-L12, rain gauge TE525-L, CR1000 data storage system). Campbell Sci ®). The deviations of the low-cost sensors were estimated in relation to those of the standard sensor and the commercial sensor. In addition, the ETo estimation was performed with theoretical solar radiation

data *via the Hargreaves–Samani model* (Equation (4)), which, despite being initially recommended for use in arid regions, was parameterized by Borges *et al.* (2010) for the city of Cruz das Almas, Bahia.

$$Rs = K_{Rs}\,(T_{max} - T_{min})^{0,5} Ra \qquad (4)$$

where Rs is the solar radiation calculated via the model; the K_{Rs}calibration coefficient is 0.19, as suggested by Borges *et al.* (2010), for the city of Cruz das Almas, Recôncavo region of Bahia, Brazil; the T_{max}maximum air temperature (°C)); and the T_{min}minimum temperature (°C); Rais the solar radiation at the top of the atmosphere (MJ m $^{-2}$ day $^{-1}$).

4.6 Integration of the pyranometer with a low-cost DSS

The data storage system (DSS) used during the pyranometer calibration has an internal 13-bit analog-digital converter (ADC) (CR1000 *Campbell Sci*®). To analyze the feasibility of using this sensor coupled with a low-cost data storage system, an evaluation of the HX711 ADC module was performed. For this purpose, an LP02 sensor and a low-cost pyranometer were installed in an open field, as shown in Figure 3.

Figure 3. Diagram of the comparative field experiment setup between the use of the HX711 analog/digital converter and the internal analog/digital converter of the CR1000.

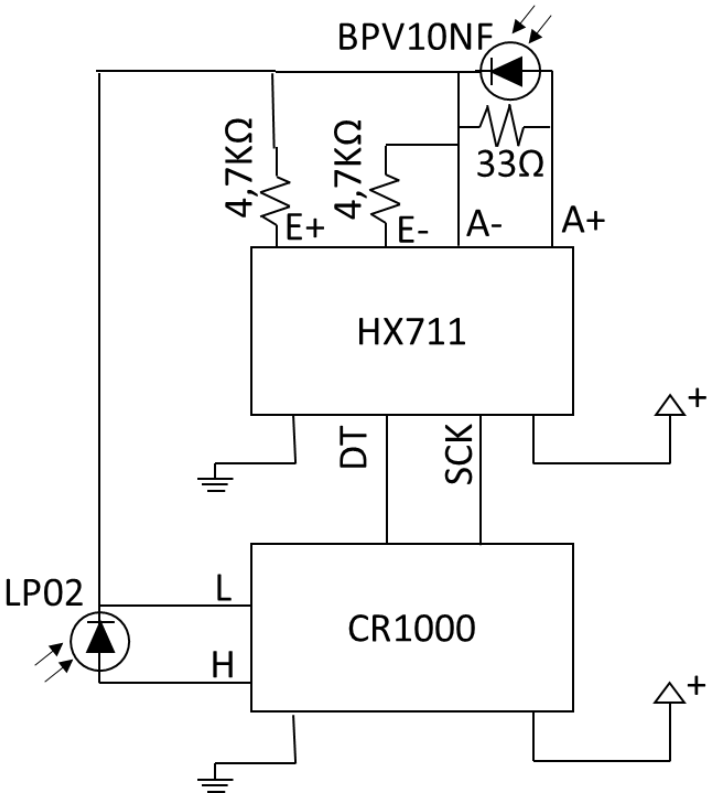

Source: The authors (2020).

The observations were carried out over a seven-day period between January 8, 2020, and January 15, 2020. The HX711 CAD is a device used to discretize an analog signal through a 24-bit digitization circuit. This easily available device was developed by *AVIA Semiconductor*® for use primarily on scales. However, it is currently widely used in a wide range of fields, as it enables

accurate results at low costs (CAQUIMBO; ROJAS; POLANCO, 2015).

5 RESULTS AND DISCUSSION

5.1 Photodiode selection

The pyranometer prototypes built with the BPW20RF and BPV10NF sensors evaluated in relation to the Campbell SC® LP02 thermal pyranometer showed high correlation coefficients $R^2 > 0.99$, with a linear increase in the signal in response to incident solar radiation. Similar results were obtained by Nwankwo, Nnabuchi, and Ekpe (2012), who reported correlation coefficients of $R^2 > 0.99$ between their homemade sensor and the standard sensor. Medugu, Burari, and Abdulazeez (2010) evaluated a pyranometer built with a BPW21 photodiode from the same line of photodiodes and with similar characteristics to those tested in the present work, obtaining an error of ±0.024 Wm^{-2} in the measured value.

According to Freire (2008), the use of PVC materials, such as those adopted in this research (glove and caps), acts as a filter for shortwave radiation and protects the internal elements of the sensor against the influence of ambient temperature due to the low thermal conductivity of the material (0.23 $W\ m^{-1}\ ^{\circ}K^{-1}$). The black color in the sensor reduces the reflection of light by the inner wall of the glove, as observed by Bolzan (2014), who coated the body of his homemade pyranometer prototype with black material, resulting in improved sensor performance.

From the observations in the open field, the pyranometer built with the BPW20RF photodiode presented a maximum signal amplitude of 1.045 mV, and the pyranometer built with the BPV10NF sensor presented a maximum signal of 0.7813 mV. For both proposed sensors, the probability of deviations occurring was less than ± 0.043 MJ m^{-2} in 95% of the measurements, with a maximum deviation of ± 2.21% and a minimum deviation of ± 0.11%.

The relative error was greater for BPW20RF (± 1.73%) than for BPV10NF (± 0.694%), but it was lower in both cases than that of the commercial CS300 sensor, ± 5% for total daily radiation (according to the manufacturer). The deviation values are in agreement with the observations of Freire (2008), who estimated the daily difference at ± 2% of the global radiation measured with a homemade photovoltaic pyranometer prototype and a commercial pyranometer of the brand *Eppley* ®.

The acquisition cost of the BPV10NF photodiode on the market is lower than that of the BPW20RF photodiode. Given the above and considering the lower relative error, greater linearity with respect to variations in ambient temperature between 0°C and 40°C (VISHAY, 2019), greater saturation amplitude (VISHAY, 2019), and lower acquisition cost on the market, the BPV10NF photodiode was selected for use in the construction of 16 photovoltaic pyranometers. These were calibrated and subjected to tests to evaluate their ability to estimate ETo_{PM}.

5.2 Sensor Calibration

On average, the 16 sensors were able to adequately represent daytime irradiance, with a sensitivity between 0.15 and 0.25 µV $W^{-1}\ m^{-2}$ for irradiance values up to 1108 W m^{-2} (Figure 4). The average signal amplitude in the sensors was 0.33 mV when evaluated in an open field and 0.35 mV when evaluated in a protected environment. Thus, the sensor's operating voltage is below the saturation limit of 450 mV for the BPV10NF photodiode (VISHAY, 2019). Accordingly, the sensors can operate both in an open field and in a protected environment without presenting a risk of saturation.

Figure 4. Time course of solar radiation for the days corresponding to the winter and summer solstices and equinox that occurred during the sensor calibration period under open field conditions between 04/13/2018 and 06/01/2019 in the municipality of Cruz das Almas, BA.

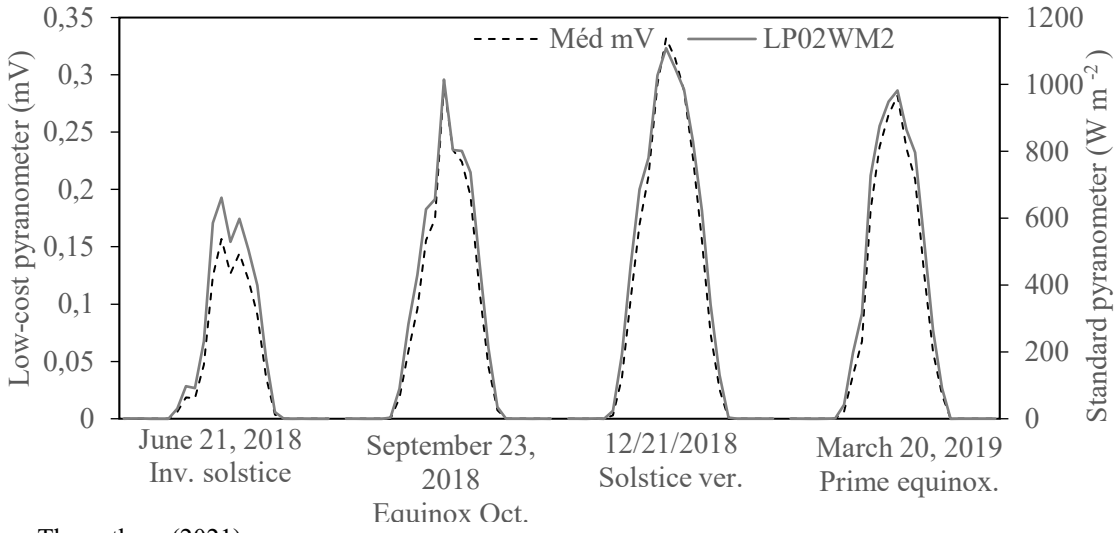

Source: The authors (2021).

The average radiation observed by the 16 sensors over a one-year period (Figure 5) exhibited wave-like behavior as the seasons progressed. The sensitivity was low in autumn and increased as spring approached. The peak values occurred between spring and summer and decreased again in autumn, with an apparent minimum occurring between autumn and winter. This behavior is attributable to a quadratic signal.

The greater sensitivity during the spring and summer months may be influenced by the high temperatures and low cloud cover characteristic of the season, a phenomenon observed by Čekon, Slávik, and Juras (2016), who attributed the variations in signal gain to the increase in diffuse radiation on days with cloudy skies and occasional rain. On the day with the lowest maximum radiation recorded, approximately 600 W m-2 (Figure 4), which corresponded to the winter solstice (June 21, 2018), 6.3 mm of precipitation, 90.7% relative humidity, and the lowest maximum temperature of the year, 21.8°C, were recorded. During this day, the sensors generally showed a drop in the voltage response. One possible cause is the formation of a water layer on the flat surface of the sensor, limiting the radiation spectrum that reaches it.

Figure 5. Variation in signal sensitivity (μV W $^{-1}$ m ^{2}) over a year marked by the climatic seasons (autumn, winter, spring and summer) during the evaluation period of the sensors under open field conditions between 04/13/2018 and 06/01/2019 in the municipality of Cruz das Almas, BA.

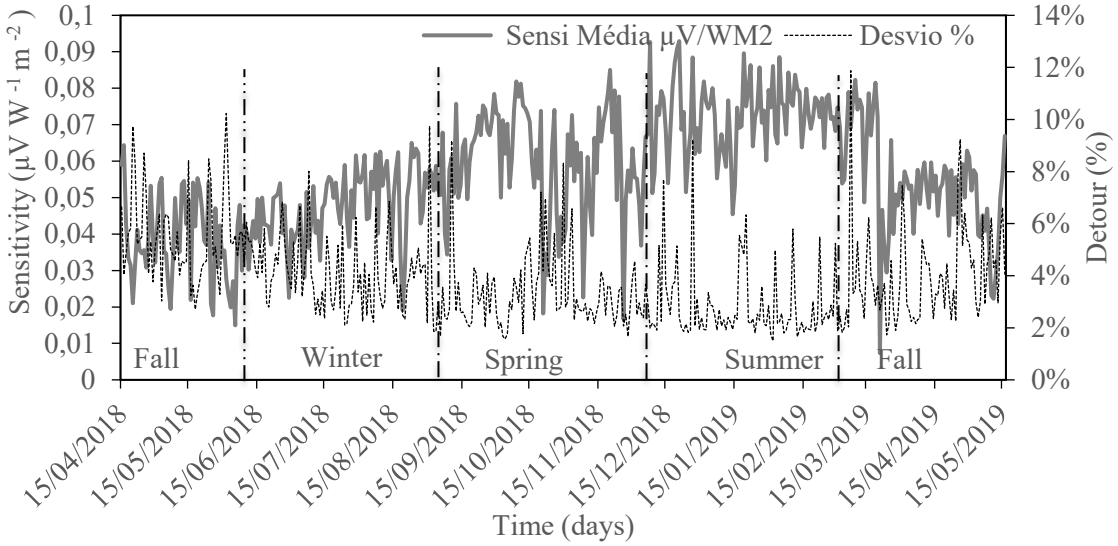

Source: Author (2021).

Differences in pyranometer sensitivity are caused by material handling during the assembly process, which requires individual calibration. Notably, even industrially manufactured radiation sensors are individually calibrated.

The calibration equations were obtained from the relationship between the daily accumulated signal (mV) and the total daily irradiance values (W m $^{-2)}$. The irradiance values were then expressed as energy on a daily scale (MJ m $^{-2}$ day $^{-1}$) (GÓMEZ *et al.*, 2018). The mathematical relationship that presented the best fit for sensor calibration, in terms of the correlation between the irradiance and electrical signal, was a second-degree polynomial equation (Equation 5). The equation was used for all sensors with specific coefficients, both for the open field and the protected environment.

$$Irradiância = a * (sinal\,mV)^2 + b * (sinal\,mV) + c \quad (5)$$

where a, b, and c are the model coefficients and the mV signal refers to the observations made with each sensor.

The average deviation for the open field measurement (σ= ± 0.048 MJ m $^{-2}$ day $^{-1}$) was slightly greater than the average deviation presented by the sensors in a protected environment (σ= ± 0.041 MJ m $^{-2}$ day $^{-1}$). For the open field condition, the average relative error over the one-year period was 3.79%, and the average absolute error was 0.79 MJ m $^{-2}$ day $^{-1,}$ varying, depending on the day of the year, between 5.2 and 0.06 MJ m $^{-2}$ day $^{-1}$. The largest errors occurred in the autumn–winter period (5.2%). In the protected environment condition, the average absolute error was 0.37 MJ m $^{-2}$ day $^{-1,}$ and the average relative error was 0.24%, which indicates that, on average, the sensors make fewer errors in a protected environment than in an open field condition, probably due to the greater diffuse radiation and absence of rain.

The physical conservation status of the pyranometers was maintained during the

414-day period, remaining intact without any visible changes during the study, both in the open field and in a protected environment. No tendency for deviations to increase over time was observed, indicating the stability of the optical properties of the materials used. The average uncertainty of the instruments for a 95% probability of deviation occurrence is 1.88 MJ m $^{-2}$ day $^{-1}$ for use in the open field and 0.94 MJ m $^{-2}$ day $^{-1}$ for use in a protected environment (Figure 6). With a 99.7% confidence interval, the minimum number of observations required to define the number of days required for calibration of the sensors with an average deviation of 2 MJ m $^{-2}$ day $^{-1}$ is estimated at 32 days (Equation 2).

Figure 6. Mean deviation for 95% of the measurements of global mean solar radiation estimated with the 16 low-cost pyranometers built with the BPV10NF photodiode in the municipality of Cruz das Almas, BA. (A) Open field conditions (from 04/13/2018 to 06/01/2019) and (B) protected environment (from 11/01/2019 to 12/10/2019).

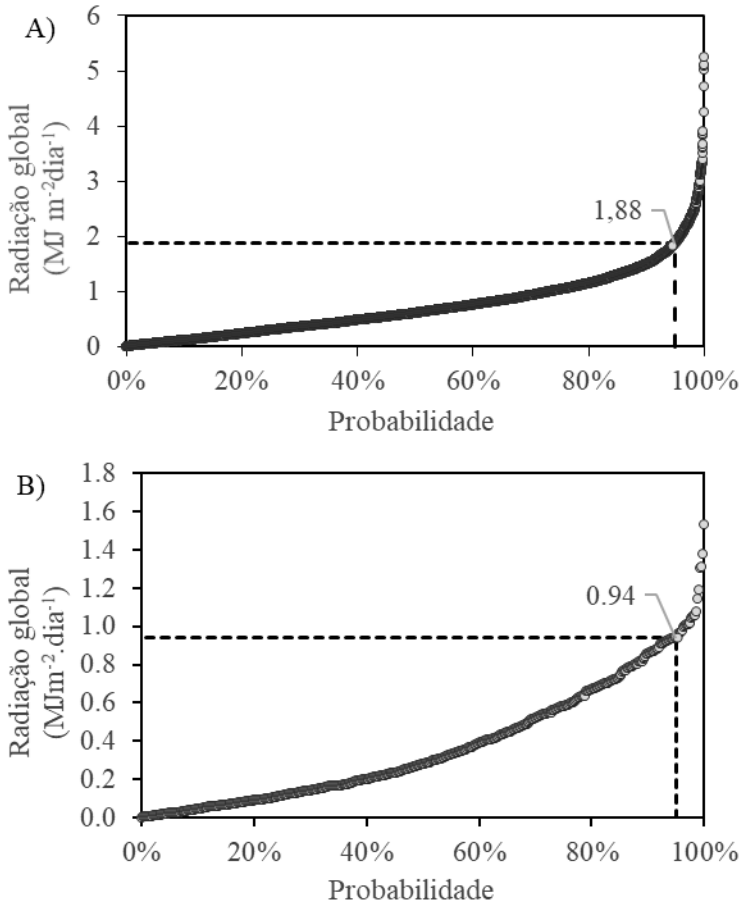

Source: The authors (2021).

5.3 Estimation of reference evapotranspiration

The reference evapotranspiration estimated with the solar radiation measured by the 16 pyranometers over 365 days of observations in the open field, with the commercial photovoltaic pyranometer, with the standard sensor, and with the global radiation estimated by the *Hargreaves–Samani model* are presented in Figure 7.

Figure 7. Daily potential evapotranspiration estimated from solar radiation measured with three different sensor types. CS300, commercial sensor; LP02, standard sensor; SP16, average of 16 low-cost pyranometer sensors; and HS *Hargreaves-Samani physical model*. The one-year period under open field conditions was between April 13, 2018, and June 1, 2019, in the municipality of Cruz das Almas, BA.

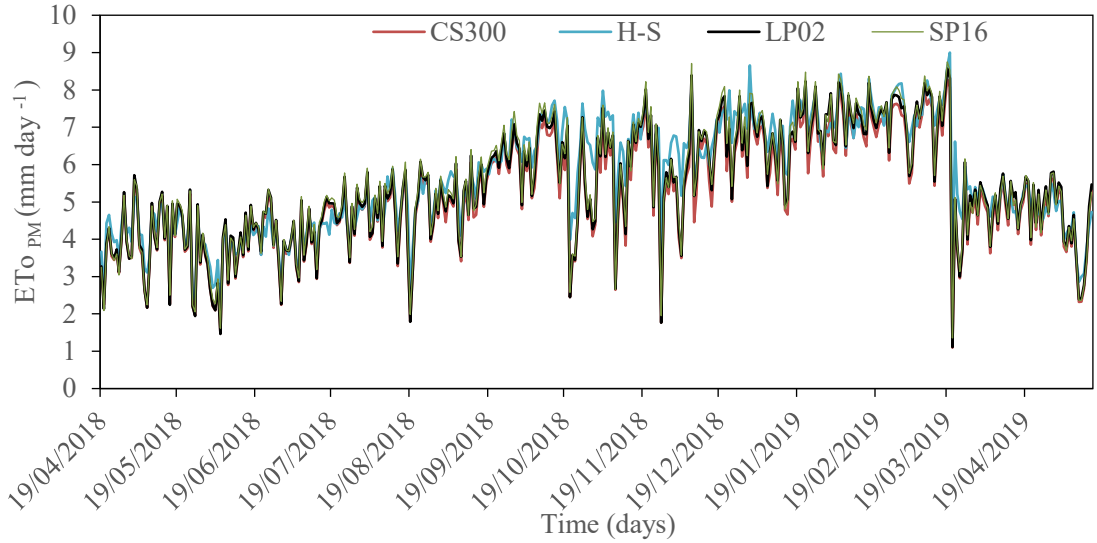

Source: The authors (2021).

The trend of the average ETo $_{PM}$ estimated from the 16 low-cost sensor prototypes tested had greater linearity (R^2 = 0.9588) than did the trend of the ETo $_{PM\ values}$ estimated *via the Hargreaves–Samani* physical model calibrated for the region (R^2 = 8471). The ETo $_{PM}$ estimated by the model had greater dispersion than the values calculated with the commercial sensor (CS300) did (Figure 8).

Figure 8. ETo $_{PM}$ linearity trend of calibrated sensors during the period from 04/13/2018--06/01/2019 under open field conditions in the municipality of Cruz das Almas, Ba. Estimated with (A) the *Hargreaves–Samani (HS) physical model; (B) the commercial CS300 sensor; (C) average of the 16 low-cost pyranometer sensors (SP16) in relation to the* ETo $_{PM}$ values estimated with the standard pyranometer LP02.

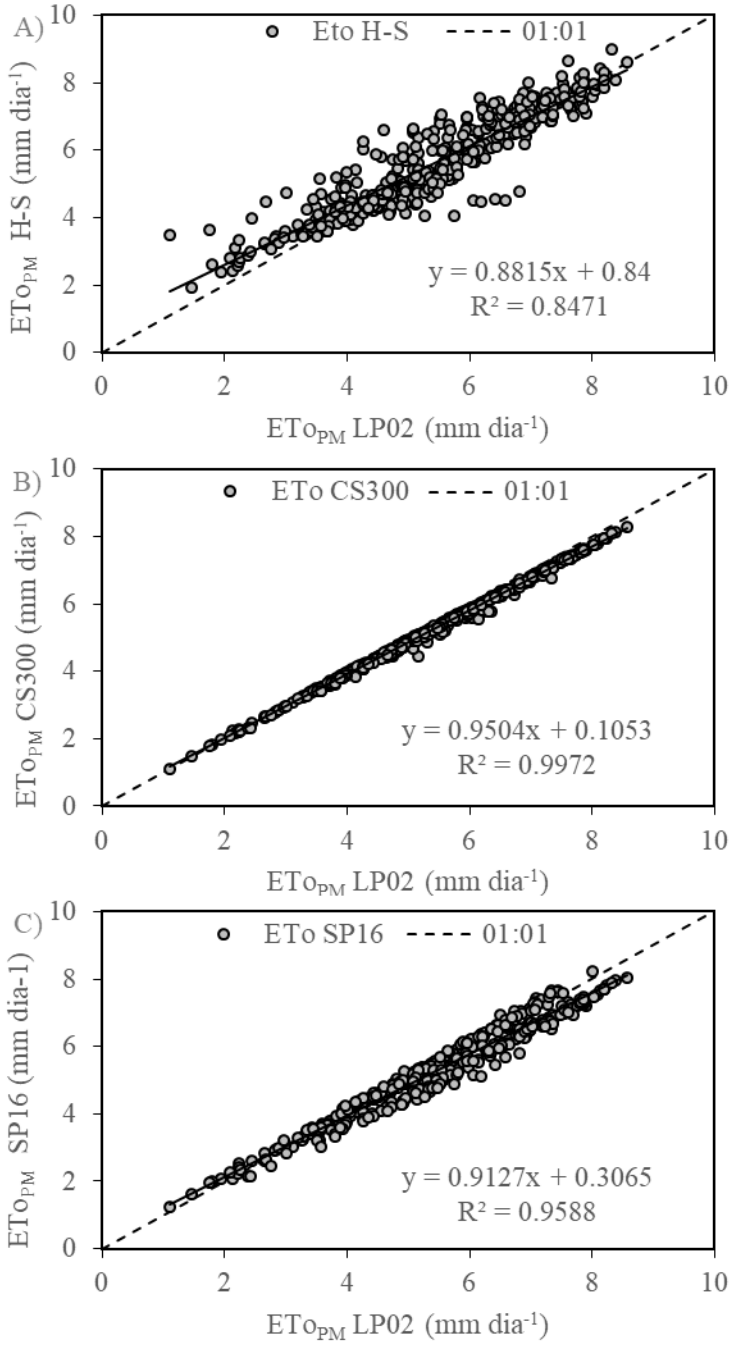

Source: The authors (2021).

Comparing the mean of the ETo $_{PM\ estimates}$ via the low-cost pyranometers against the ETo $_{PM}$ estimated via the standard pyranometer, the mean absolute deviation for the total observations was 0.16 mm day $^{-1}$, and the standard deviation was ± 0.22 mm day $^{-1}$ for 95% of the observations, which is equivalent to a mean percentage deviation of 3%.

These indicators are 3.62 times smaller than those estimated *via the Hargreaves–Samani model*, which were 0.58 mm day $^{-1}$ for the mean absolute deviation and 0.55 mm day $^{-1}$ for the standard deviation. In one year of measurement, the ET estimated by the *Hargreaves-Samani model*, which, even with local calibration, presented an absolute cumulative error (183.94 mm) greater than the absolute cumulative error when the ET was calculated via the low-cost pyranometer and the commercial CS300 sensor, presented an absolute cumulative error of 65.64 mm, compared with the ETo $_{PM}$ estimated with the standard LP02 sensor. Therefore, when *the Hargreaves–Samani model is used*, the use of low-cost sensors previously calibrated to local conditions is a viable and advantageous option for estimating ETo, integrating these sensors into an EMA.

5.4 Pyranometer test associated with readings of the HX711 Analog to Digital Converter

Using the CAD HX711 to measure the pyranometer proved to be an accurate alternative, since the estimated relative uncertainty for 95% of the measurements is less than ± 0.86 µV (Figure 9), which is lower than the accuracy indicated by the manufacturer of the CAD CR1000 (*Campbell SC*®), which in this measurement range (2.5 mV) is ± 1.5 µV. The HX711 can measure the voltage values generated in the photovoltaic pyranometer with a resolution of ± 0.002 µV and complete linearity in relation to the commercial CAD (y = 1.0007x + 0.0006; R ^{2} > 0.9999). This deviation corresponds to an error in the radiation estimate of 1.8 MJ m $^{-2}$ day $^{-1}$ and 0.22 mm day $^{-1}$ in the reference evaporation.

Figure 9. Estimated relative uncertainty for 95% of the measurements performed with the HX711 analog-to-digital converter, evaluated via an LP02 pyranometer in an open field over a 7-day period (from 01/08/2020 to 01/15/2020) in the municipality of Cruz das Almas, BA.

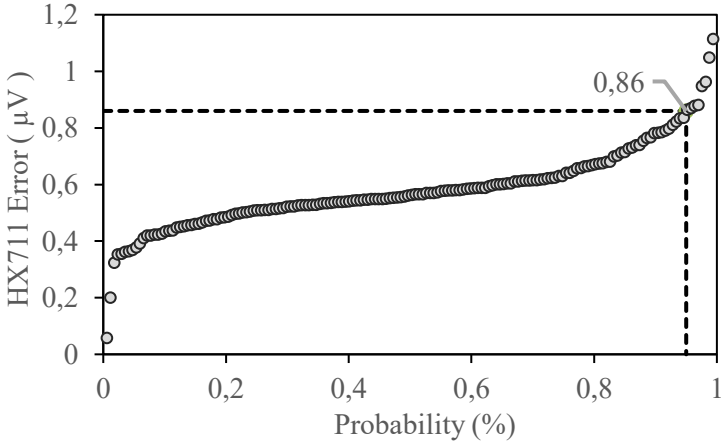

Source: The authors (2021).

5.5 Construction costs

The approximate production cost of the pyranometer for 2021 was R$136.17, or US$27.23, on the basis of the average dollar price in May 2021. These values are lower than those available on the market with similar operating characteristics. For example, the model built with a silicon cell from the Apogee® brand, whose estimated price was US$337.00, and even those developed with the purpose of reducing costs in relation to commercial models, such as the sensor developed by Freire (2008), whose cost corresponded to US$150.00, according to the author.

The pyranometers were constructed using readily available components from the local market. According to the 2021 data presented in Table 1, these components can cost approximately R$30.00. Sensor fabrication can take approximately three hours and cost approximately R$10 per hour, resulting in a total cost of R$30.00 per sensor.

To ensure proper sensor operation, it is important to calibrate the sensors via a secondary standard thermopile pyranometer such as the LP02 or similar. The price of the LP02 standard pyranometer is US$983.25. Considering a useful life of up to 10 years and a 12% capital cost, calibration for a 32-day period costs R$42.17. During this calibration process, it is important to have qualified personnel install the sensors, supervise them, and perform subsequent calculations. This work costs approximately R$34 for 4 hours of work.

Table 1 Production cost of the artisanal pyranometer.

Item	Value R$	Value US$
Components	30.0	6.0
Construction workforce	30.0	6.0
Calibration workforce	34.0	6.8
LP02 Standard Sensor Rental	42.17	8.43
TOTAL VALUE	136.17	27.23

Source: The authors (2021).

6 CONCLUSIONS

The pyranometer construction methodology was easy to reproduce because of its use of low-cost, commercially available materials. The sensors, subjected to field conditions for 414 days, showed no physical deterioration, and the estimated data were in agreement with the seasonal course of the standard sensor time series. Estimating ETo $_{PM}$ via solar radiation measured by the constructed pyranometers and recording the data via the HX711 converter demonstrated that this sensor can be used in automated weather stations, which are installed in open fields or protected environments, with sufficient accuracy for reliable and low-cost estimates of reference evapotranspiration via the *Penman model. Montheith* .

7 ACKNOWLEDGMENTS

The authors thank CAPES for the scholarships and CNPq for financing this research through project 409332/2018-6.
This article is derived from the master's dissertation Sánchez-Benítez, J. Low-cost sensors for continuous monitoring of soil moisture and solar radiation. Federal University of Recôncavo da Bahia. 2021.

8 REFERENCES

ALLEN, RG; PEREIRA, LS; RAES, D.; SMITH, M. **Crop evapotranspiration** - guide lines for computing crop water requirements. Rome : FAO, 1998. (Irrigation and Drainage paper, 56).

BOLZAN, MB **Development of a pyranometer based on semiconductor components** . 2014. Dissertation (Master in Metrology) – Universidade Federal de Santa Maria , Santa Maria, Brazil, 2014.

BORGES, VP; OLIVEIRA, ASD; COELHO FILHO, MA; SILVA, TS; PAMPONET, BM Evaluation of models for estimating incident solar radiation in Cruz das Almas, Bahia. **Brazilian Journal of Agricultural and Environmental Engineering** , City: Campina Grande, Paraíba, Brazil, v. 14, n. 1, p. 74-80, 2010.

BORNHOFEN, E. Evapotranspiration of FAO crop 56. **Tropical Agricultural Research** , City: Goiânia, Goiás, Brazil, v. 45, n. 1, p. 46-55, 2015.

CAMPBELL SCIENTIFIC. **CS300 Silicon Pyranometer** . City: North Logan, Utah, USA, Publisher: Campbell Scientific , Inc., 2018. Available at: https://www.campbellsci.com/cs300-pyranometer. Accessed on: May 15, 2021.

CAMPBELL SCIENTIFIC. **LP02 pyranometer Sensor** . City: North Logan, Utah, USA, Publisher: Campbell Scientific , Inc. , 2012. Available at: https://www.campbellsci.com/lp02-l . Accessed on: May 15, 2021.

CAQUIMBO, CCP; ROJAS, RQ; POLANCO, JDQ Design and implementation of a medical prototype for him treatment and control of Diabetes Mellitus Type 1. **Engineering and Region** , City: Neiva, Huíla, Colombia, H v. 13(1), p. 191-200, 2015.

CEKON, M.; SLÁVIK, R.; JURAS, P. Obtainable method of measuring the solar radiant fluxbased on silicon photodiode element . **Applied Mechanics and Materials** , City: Schweiz , Switzerland, v. 824, p. 477–484, 2016.

FREIRE, LAD **Development of a photovoltaic pyranometer** . 2008. Dissertation (Master in Energy and Nuclear Technologies) – Federal University of Pernambuco , Recife, Brazil, 2008.

GÓMEZ, JM; CARLESSO, F.; VIEIRA, LE; SILVA, L. Solar irradiance: basic concepts. **Brazilian Journal of Physics Education** , City: São Paulo, São Paulo, Brazil, v. 40, n. 3, p. e3312-1-e3321-12, Mar. 2018.

INMETRO. **Evaluation of measurement data** - Guide to the expression of measurement uncertainty - GUM 2008. City: Rio de Janeiro, Rio de Janeiro, Brazil, 2012a.

INMETRO. **International Vocabulary of Metrology** : VIM 2012. Fundamental and general concepts and associated terms. 1st ed. City: Rio de Janeiro, Rio de Janeiro, Brazil, INMETRO, 2012b.

INTERNATIONAL ORGANIZATION FOR STANDARDIZATION. **ISO 9060: 1990 -** Solar Energy - specification and classification of instruments for measuring hemispherical solar and direct solar radiation. ISO, City: Geneva, Switzerland , 1990.

MAPA. National Institute of Meteorology. **Inmet automatic meteorological station network** . Brasília, DF: MAPA, 2011. (Technical note no.

001/2011/SEGER/LAIME/CSC/INMET). Available at: http://www.cemtec.ms.gov.br/wp-content/uploads/2019/02/Nota_Tecnica-Rede_estacoes_INMET.pdf. Accessed on: October 29, 2020.

MEDUGU, D.; BURARI, F.; ABDULAZEEZ, A. Construction of a reliable model pyranometer for irradiance measurements. **African journal of Biotechnology, Academic Journals** (Kenya), v. 9, no. 12, 2010.

NWANKWO, SN; NNABUCHI, MN; EKPE, JE Construction and characterization of a pyranometer using locally available materials for global solar radiation measurement. **Asian Transactions on Basic and Applied Sciences** , City: Pakistan , v. 26, n. 4, p.26-33, 2012.

RAFI, Z; MERLIN, O; LE DANTEC, V.; KHABBA, S.; MORDELET, P.; ER-RAKI, S. FERRER, F. Partitioning evapotranspiration of a drip-irrigated wheat crop: Intercomparing eddy covariance-, sap flow-, lysimeter- and FAO-based methods. **Agricultural and Forest Meteorology** , City: Guelph , Ontario, Canada, v. 265, p. 310-326, 2019.

SILVA. EA **Parameter estimation techniques for photovoltaic modules** . Dissertation (Master's in Electrical Engineering) – Federal University of Pernambuco , Recife, 2015.

VILELA, WA **Study, development and characterization of radiometers for measuring solar radiation** . 2010. Theses (Doctorate in Engineering and Technology Space/Science and Technology Materials and Sensors) – National Institute for Space Research , São José dos Campos, 2010.

VISHAY. **Silicon PIN Photodiode** . BPV10. Vishay , 2019. Available at: www.vishay.com/docs/81502/bpv10.pdf . 2019. Accessed on: October 29, 2020.

VISHAY. **Silicon Photodiode , RoHS Compliant .** BPW20RF . Vishay , 2011. Available at: www.vishay.com/docs/81570/bpw20rf.pdf. 2011 . Accessed on: October 29, 2020.